A Comparative Study Between Dielectric and Microstrip Antenna Arrays for GPS Application

Gabriel P. Paulena, Herick R. da S. Rodrigues, Edson R. Schlosser and Marcos V. T. Heckler

***Abstract*— This paper presents the performance comparison between a top-loaded circular dielectric resonator antenna (TLCDRA) and a microstrip antenna (MSA), both designed to operate at GPS L1-Band (centered at 1.575 GHz). The TLCDRA is excited by cross-rectangular slots to achieve circular polarization, while the MSA uses a coaxial probe along the patch diagonal. Then, the antennas are arranged in a 2×2 planar array with two inter-element spacings: $0.5\lambda_0$ and $0.4\lambda_0$. In order to assess the performance of the proposed arrays, a study on the beam steering scenarios are simulated, and the resulting radiation patterns, including gain and axial ratio characteristics, are analyzed and discussed.**

***Keywords*— Cylindrical Dielectric Resonator Antenna, Microstrip antenna, Low profile antennas, GPS.**

I. Introduction

Nowadays, there has been an increase in ecological awareness within Society. As a result, various projects have emerged to monitor environmental variables such as temperature, atmospheric pressure, carbon dioxide levels in the air, ultraviolet radiation, rainfall, among others. In order to accurately diagnose environmental conditions, it is necessary to continuously collect the meteorological data mentioned above. For terrestrial monitoring, data collection platforms (DCPs) are installed in different geographical areas to collect environmental data [1]. For offshore data collection, DCPs can be installed on sea buoys to monitor oceanic and atmospheric conditions [2]. To ensure accurate weather forecast, these DCPs rely on the Global Navigation Satellite System (GNSS) to determine the geographic position, which is particularly important in the case of offshore data acquisition, since the sea buoys may change their position due to the ocean streams and wave motion.

The GNSS works by transmitting and receiving electromagnetic waves in frequency bands around 1.2 and 1.6 GHz, allowing for the use of more compact equipment to receive the signals. Another advantage is its robustness against atmospheric attenuation, due to signal transmission in the microwave range. The main regional or global positioning systems, developed by various countries to ensure independence and autonomy in the acquisition of georeferenced data, include GPS (Global Positioning System), GLONASS (from Russian, *Global'naya Navigatsionnaya Sputnikovaya Sistema*), BeiDou (Big Dipper), and Galileo [3].

An essential requirement for reliable GNSS operation is the use of circularly polarized antennas (CP) due to their capability of receiving signals with arbitrary electric field orientations and also to minimize losses caused by polarization mismatch between the incident wave and the receiving antenna [4]. The requirements for an ordinary GPS antenna are generally: gain in the range of 3 to 5 dBic, bandwidth of 20.046 MHz in the L1-Band and 20.46 MHz in both L2 and L5-Bands, and right-hand circular polarization (RHCP) [3]. Different types of antennas can be used to receive signals from this system, with dielectric (DRA) and microstrip (MSA) antennas standing out as prominent options [5], [6].

Microstrip antennas are widely used due to their ease of fabrication, low cost, compact size and low-profile aspect. However, some limitations are related to moderate radiation efficiency and mechanical fragility [7], [8]. On the other hand, DRAs are particularly attractive for operation at microwave frequencies, due to the minimal use of conductive materials in their physical construction. Moreover, there is no excitation of surface waves, which results in low losses and, consequently, increases the antenna radiation efficiency. The materials used to build such an antenna offers more mechanical robustness [9]. Nonetheless, to achieve compact and low profile designs, high dielectric constant materials and miniaturization techniques are normally employed, which yield narrow operational bandwidth and high cost.

These two antenna types have close similarity regarding their feeding mechanisms and radiation patterns. Although each type offers distinct advantages, few works have focused on a direct performance comparison between the DRA and MSA. In [10], a performance comparison between two arrays operating at 25 GHz, one composed of DRAs and the other of MSA, is reported. In [11], the authors compare the radiation efficiency of DRA and MSA, both designed to operate in Ka-Band with center frequency at 35 GHz. Similarly, in [12], the performance of a cylindrical DRA and a circular MSA operating in X-Band is presented. However, to the best of the author's knowledge, no prior work reports a performance comparison between DRA and MSA designs at GNSS bands.

In this context, the present work provides a direct performance comparison between DRA and MSA, both designed to operate in the GPS L1-Band, centered at 1.575 GHz. In addition, to extend the analysis beyond single element performance, each antenna type is used to compose 2×2 arrays for parameters investigation, such as radiation pattern, sidelobe levels (SLL) and cross-polarization discrimination (XPD). This kind of study offers valuable insights on their suitability to be used in GNSS applications.

The paper is organized as follows: section II presents the DRA and MSA designs in detail. The comparison of the

Gabriel P. Paulena, Herick R. da S. Rodrigues, Edson R. Schlosser and Marcos V. T. Heckler, Laboratório de Eletromagnetismo Microondas e Antenas (LEMA), Universidade Federal do Pampa (UNIPAMPA), Alegrete-RS, e-mail: gabrielpaulena.aluno; herickrodrigues.aluno; edsonschlosser; marcosheckler@unipampa.edu.br.

performance of both array types is discussed in section III. Finally, section IV provides the conclusions drawn from this work.

II. Design and Performance Analysis of DRA and MSA Antennas

The antennas geometries to be compared consist of a cylindrical DRA and a square MSA. Both were designed and simulated in HFSS. The design process for each antenna was carried out to operate at the same center frequency (1.575 GHz), allowing a comparison of key parameters such as gain, bandwidth, and radiation pattern. Detailed descriptions of the design process, including material selection, dimension optimization, and excitation, are described in the following subsections.

A. Cylindrical DRA Design

Low-profile DRAs can be achieved by employing miniaturization techniques to reduce their physical dimensions. In [13], a proposed miniaturization technique involves applying a metallic layer to the top of a cylindrical dielectric resonator antenna (CDRA) to reduce the wavenumber in the z-direction, resulting in a more compact geometry. Considering a thin cylindrical structure, the analyzed geometry exhibits the TM^z_{mnp} mode. As the insertion of the metallic load reduces the wavenumber in the z-direction to zero (p = 0), the antenna radius can be written in terms of the resonance frequency as

$$a = \frac{1}{2\pi\sqrt{\mu\varepsilon}}\left(\frac{\chi'_{mn}}{f_{r_{mn}}}\right), \tag{1}$$

where μ is the magnetic permeability, ε is the electric permittivity, χ'_{mn} corresponds to the mn-th root of the derivative of the Bessel function and $f_{r_{mn}}$ is the resonance frequency.

The main dimension that governs the resonance frequency of the fundamental mode of the top-loaded cylindrical resonator antenna (TLCDRA) is the radius, which is obtained using the lowest value of the root χ'_{mn} for m = n = 1; i.e., χ'_{11} = 1.8412. Therefore, the fundamental mode of a TLCDRA is the TM^z_{110}. Considering the resonance centered at 1.575 GHz, the analytical radius calculated using (1) yields a = 17.64 mm.

To compensate the narrow impedance bandwidth effects, the TLCDRA investigated in this work is designed with two stacked layers of CER-10 laminate (ε_r = 10, loss tangent $\tan\delta$ = 0.0035) and a metallic load with thickness of 35 μm. The laminates are bonded using one layer of prepreg Fast Rise 27 (FR-27-0035-66), which has dielectric constant of ε_r = 2.7, loss tangent of $\tan\delta$ = 0.0017 and thickness of 45 μm. Consequently, the total cavity height of the antenna is h = 6.44 mm. For the ground plane (GND), a double-sided FR4 laminate with 35 μm thick copper layers and dimensions of 95×95×1.524 mm was used. The electromagnetic properties of this laminate are ε_r = 4.4 and loss tangent of $\tan\delta$ = 0.02.

The TLCDRA is centrally positioned on the FR4 laminate, as illustrated in Figure 1a. In this work, the slot aperture coupling scheme proposed in [14] is used as the excitation mechanism due to its advantages, including strong electromagnetic coupling, ease of integration with printed feed structures and the capability to achieve CP. The aperture comprises two slots cut into the GND, which are fed by a microstrip line positioned beneath it, as illustrated in Figure 1b. The slots length are precisely adjusted to achieve CP configuration by means of parametric analyses carried out in HFSS. After the optimizations, these dimensions are L_{slot1} = 20.1 mm and L_{slot2} = 14 mm. To guarantee a good impedance matching, the stub dimensions are L_{stub} = 20 mm and W_f = 2.87 mm. The antenna final dimensions ($a \times h$) are 18.255 × 6.44 mm, which corresponds to 0.0958 × 0.0334 λ_0 in terms of free-space wavelength.

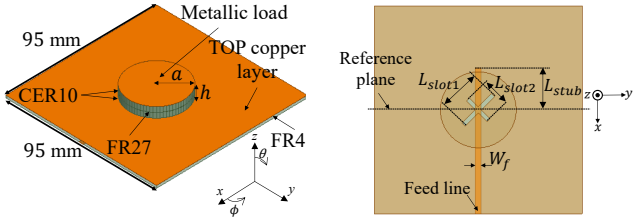

Fig. 1. TLCDRA fed by cross-rectangular slot aperture. (a) Antenna structure. (b) Feeding mechanism.

The simulated results are shown in Figure 2. The operational bandwidth, considering the criterion $|\Gamma| \leq -10$ dB, corresponds to 75 MHz, as reported in Figure 2a. In Figure 2b, the radiation pattern in the ϕ = 0° plane is shown. The antenna gain at boresight is equivalent to 5.67 dBic with a half power beamwidth of 90.48°. Regarding the cross-polarization (LHCP), the highest level appears at the boresight with −10.84 dB, which yields an XPD of 16.51 dB. In Figure 4c, the radiation efficiency as a function of frequency is presented. At 1.575 GHz, the antenna exhibits efficiency equal to 82.3%. Finally, considering an AR ≤ 3 dB, the antenna shows a beamwidth of 194.81°, as exhibited in Figure 2d.

B. Square MSA Design

The analyzed geometry chosen for MSA is presented in Figure 3a and has been proposed in [15]. This antenna consists in a square patch with edge size L excited with a single coaxial probe positioned along the patch diagonal, allowing the excitation of two orthogonal modes with 90° phase shift to yield circular polarization. A slot is introduced at the geometric center of the patch, in order to excite the two orthogonal modes. The slot dimensions are used to fine-tune the antenna axial ratio.

The same FR4 laminate used as ground plane for the TLCDRA, is employed for the MSA design. Since FR4 substrate is a material with high loss tangent ($\tan\delta$ = 0.02), it results in low radiation efficiency when used in antenna designs. To mitigate this limitation, the authors investigated the use of an air layer to enhance the antenna performance particularly in terms of radiation efficiency. By doing so, the antenna is composed of two FR4 layers with thickness of 1.524 mm each, separated by an air gap with the same FR4 thickness

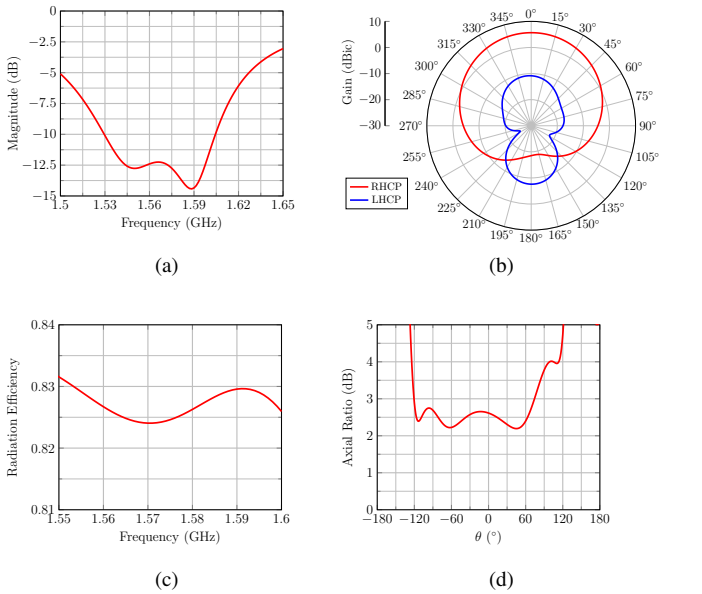

(a) (b) (c) (d)

Fig. 2. Simulated results for the TLCDRA excited with cross-rectangular slots. (a) Reflection coefficient. (b) Radiation pattern in the $\phi = 0°$ plane. (c) Radiation efficiency. (d) Axial ratio in the $\phi = 0°$ plane.

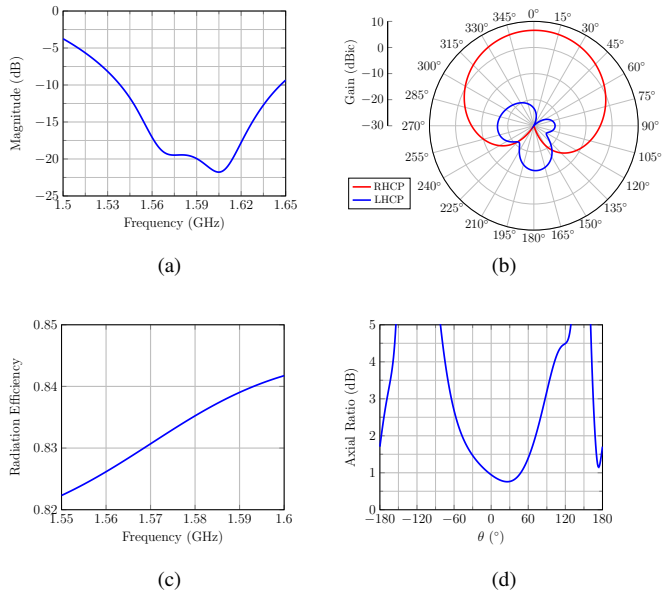

(a) (b) (c) (d)

Fig. 4. Simulated results for the MSA excited with coaxial probe. (a) Reflection coefficient. (b) Radiation pattern in the $\phi = 0°$ plane. (c) Radiation efficiency. (d) Axial ratio in the $\phi = 0°$ plane.

as illustrated in detail in Figure 3b. This procedure increases the antenna dimension in the z direction, resulting in a total height of $h = 4.572$ mm.

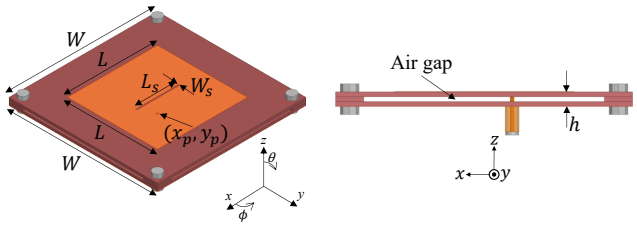

(a) (b)

Fig. 3. MSA geometry. (a) Isometric view. (b) Side view.

The antenna was initially designed using the transmission line model, followed by optimization through HFSS. The final dimensions of the antenna are: patch length L = 57.8 mm, slot length L_s = 27.25 mm, slot width W_s = 0.9 mm, and ground plane width W = 95 mm.

The simulated results are presented in Figure 4. The impedance matching was achieved by adjusting the coaxial probe position to x_p = y_p = 9 mm, yielding a reflection coefficient of -19.48 dB at 1.575 GHz and a impedance bandwidth of 110 MHz (considering $|\Gamma| \leq -10$ dB), as presented in Figure 4a. In Figure 4b, the radiation pattern in the ϕ = 0° plane is shown. The antenna gain at the boresight is equivalent to 6.64 dBic with half-power beamwidth equal to 84.22°. Regarding the cross-polarization (LHCP), it is strongly suppressed, yielding an XPD of 25.29 dB. In Figure 4c, the radiation efficiency as a function of frequency is presented, whereby it is equal to 83.3% at 1.575 GHz. Finally, considering an AR $\leq$ 3 dB, the antenna exhibits beamwidth of 151.57°, as shown in Figure 4d.

Table I summarizes the main simulated parameters for each antenna. By comparing the results, the TLCDRA exhibits a slightly narrower impedance bandwidth than the MSA. Regarding the gain in the boresight, both antennas meet the GPS gain requirement, with values above 5 dBic. The half-power beamwidth (HPBW) of the TLCDRA is wider than MSA, which favors signal reception at low elevation angles. In terms of isolation between RHCP and LHCP components, the MSA demonstrates significantly higher XPD than the TLCDRA. However, it is important to highlight that the TLCDRA offers a broader axial ratio angular width compared to the MSA, which is advantageous for GPS applications, as it indicates that the antenna can maintain circular polarization and receive signals at low elevation angles. Regarding radiation efficiency, both antennas achieve values above 80%. Finally, when analyzing the radiating element dimensions in terms of wavelength, the TLCDRA has a more compact geometry, making it particularly suitable for applications requiring miniaturization, such as embedded systems onto aerospace platforms, where the available space is limited and compact designs are essential.

TABLE I
COMPARISON BETWEEN TLCDRA AND MSA PARAMETERS.

Antenna Parameters	TLCDRA	MSA
Bandwidth ($\|\Gamma\| \leq -10$ dB)	75 MHz	110 MHz
RHCP broadside gain	5.67 dBic	6.64 dBic
HPBW	90.48°	84.22°
XPD	16.51 dB	25.29 dB
AR angular width (AR $\leq$ 3 dB)	194.81°	151.57°
Radiation efficiency	82.4%	83.3%
Dimension (λ_0)	0.09×0.03	0.30×0.02

III. 2 × 2 Planar Array Analysis

To ensure greater efficiency in GPS signals reception, antenna arrays can be employed, enabling an increase in the axial ratio beamwidth, higher gain, and changes in the radiation pattern shape through the application of beamforming techniques. In this section, the designed DRA and MSA are arranged in 2×2 planar arrays with sequential rotation, as illustrated in Figure 5. Initially, the elements of each array are linearly spaced with a center-to-center distance of $d_x = d_y = 95.2$ mm, which corresponds to $0.5\lambda_0$. Subsequently, the spacing is reduced to $0.4\lambda_0$ ($d_x = d_y = 76.19$ mm) in order to analyze the arrays performance in a more compact design.

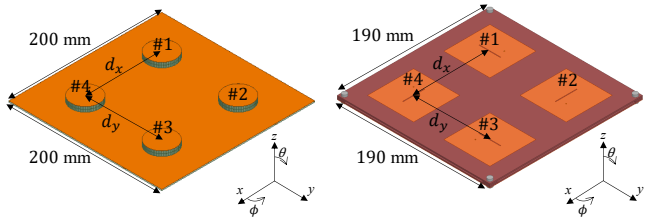

Fig. 5. 2×2 Planar antenna arrays. (a) TLCDRA. (b) MSA.

Figure 6 presents the simulated gain patterns for each array as the element spacing is varied. As the elements are placed closer together, the broadside gain tends to decrease. For the array composed of TLCDRA elements, the broadside gain drops from 10 dBic to 8.68 dBic. For the array composed of MSA elements, the broadside gain decreases from 10.6 dBic to 9.76 dBic. However, it is important to highlight that the RHCP gain patterns become less directive in both cases, resulting in a wider half-power beamwidth and reduced cross-polarization levels.

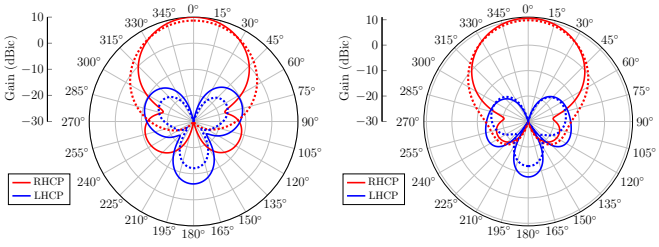

Fig. 6. Radiation pattern gain in the $\phi = 0°$ plane. (a) TLCDRA. (b) MSA. Solid lines: $d_x = d_y = 0.5\lambda_0$. Dotted lines: $d_x = d_y = 0.4\lambda_0$.

To evaluate the performance of each antenna array, different beamforming scenarios have been considered by steering the main lobe of the array towards six distinct directions. This has been achieved by exciting the antennas with uniform amplitude and progressive phase shift. Table II summarizes the gain (G) and the XPD at each steering direction, along with the angle for axial ratio lower than 3 dB. Figures 7 and 8 illustrate the gain patterns for the analyzed beam steering cases for interelement spacings of $0.5\lambda_0$ and $0.4\lambda_0$, respectively.

Based on the analyzed data, it is observed that for the TLCDRA antenna array with reduced element spacing, the

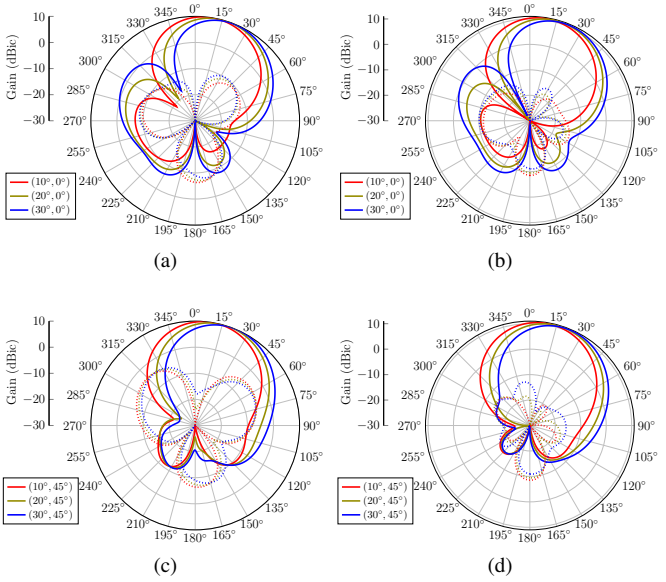

Fig. 7. Radiation pattern at 1.575 GHz for arrays with elements spaced by $0.5\lambda_0$. (a) and (c) TLCDRA array patterns. (b) and (d) MSA array patterns. Solid lines: RHCP. Dotted lines: LHCP.

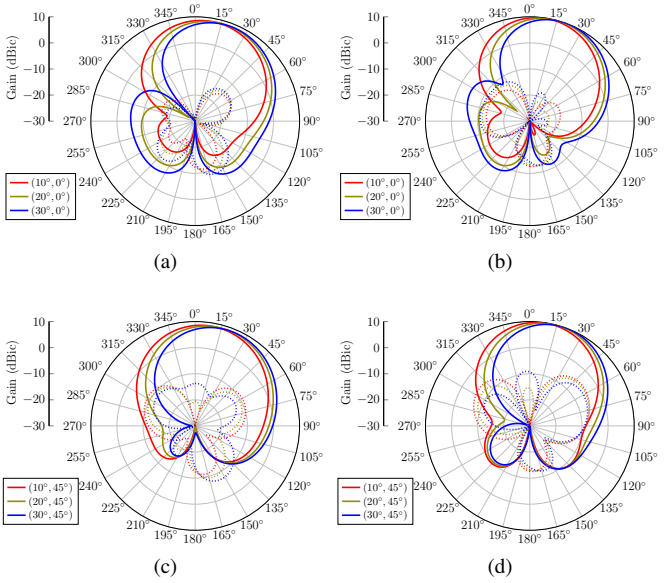

Fig. 8. Radiation pattern at 1.575 GHz for arrays with elements spaced by $0.4\lambda_0$. (a) and (c) TLCDRA array patterns. (b) and (d) MSA array patterns. Solid lines: RHCP. Dotted lines: LHCP.

gain in the steering direction decreases; however, the axial ratio beamwidth is significantly increased. Moreover, at low elevation angles ($\theta = 75°$), the array gain remains above 0 dBic, which is a very important trait for GPS signal reception, since the positioning accuracy may be increase, if satellites at low elevation angles can be efficiently tracked. The same behavior can be observed for the array composed of MSAs; however, for beam steering cases in the $\phi = 45°$ plane, the angular width of axial ratio is considerably reduced. It is important to highlight that the XPD in the main lobe directions is higher than 19 dB for all tested scenarios, hence indicating an axial ratio below 1.95 dB.

TABLE II
PERFORMANCE COMPARISON BETWEEN TLCDRA AND MSA ARRAY.

Steering Cases	TLCDRA						MSA					
$(\theta_{max}, \phi_{max})$	G (dBic)		XPD (dB)		AR angular width (AR $\leq$ 3 dB)		G (dBic)		XPD (dB)		AR angular width (AR $\leq$ 3 dB)	
	$0.5\lambda_0$	$0.4\lambda_0$	$0.5\lambda_0$	$0.4\lambda_0$	$0.5\lambda_0$	$0.4\lambda_0$	$0.5\lambda_0$	$0.4\lambda_0$	$0.5\lambda_0$	$0.4\lambda_0$	$0.5\lambda_0$	$0.4\lambda_0$
$(10^\circ, 0^\circ)$	10.00	8.70	34.11	45.55	74.83°	113.62°	10.62	9.82	38.87	41.35	103.80°	109.60°
$(20^\circ, 0^\circ)$	9.94	8.68	23.95	29.13	76.64°	161.44°	10.59	9.85	30.06	32.20	110.37°	123.89°
$(30^\circ, 0^\circ)$	9.59	8.50	19.73	24.18	80.18°	154.51°	10.25	9.64	25.99	28.28	106.35°	125.48°
$(10^\circ, 45^\circ)$	10.00	8.72	38.29	43.25	53.07°	77.15°	10.00	9.81	47.77	36.88	131.23°	60.02°
$(20^\circ, 45^\circ)$	10.00	8.78	27.13	30.64	53.22°	87.50°	10.64	9.82	40.32	26.98	121.28°	67.27°
$(30^\circ, 45^\circ)$	9.86	8.60	21.47	25.85	53.06°	131.62°	10.45	9.58	33.12	22.71	100.67°	51.73°

IV. CONCLUSION

This paper presented the design and a performance analysis comparison between a top-loaded cylindrical dielectric resonator antenna (TLCDRA) and a microstrip patch antenna (MSA), both designed to operate at the GPS L1-Band centered at 1.575 GHz. Aiming at a low profile DRA design, miniaturization technique was implemented, resulting in a compact element with dimensions $(a \times h) = 0.09\lambda_0 \times 0.03\lambda_0$. The MSA was designed using two FR4 layers separated by an air gap to improve radiation efficiency, yielding an antenna with dimensions $(L \times h) = 0.30\lambda_0 \times 0.02\lambda_0$. The simulated results demonstrate that both antennas are suitable for effective GPS signal reception. In scenarios where space constraints are more critical, the TLCDRA emerges as a strong candidate due to its compactness. On the other hand, the main advantage of the proposed approach using the MSA design is the use of only FR4, which is a low-cost laminate.

The performance of the two array configurations considering different interelement spacing was also investigated under six beam steering scenarios. The obtained results indicate that both arrays exhibit good performance, highlighting their potential for high-precision GPS applications.

ACKNOWLEDGMENT

The authors would like to thanks to the Coordenação de Aperfeiçoamento de Pessoal de Nível Superior (CAPES) (Finance Code 001) for the partial support to this research work, and Conselho Nacional de Desenvolvimento Científico e Tecnológico (CNPq) under grants 407245/2022-7, 305654/2022-5 and 406517/2022-3 (INCT-Signals).

REFERENCES

[1] W. Yamaguti, E. A. Ribeiro, J. C. Becceneri, and S. N. Itami, "Collection and treatment of the environmental data with the brazilian satellite scd1," *Revista Brasileira de Ciencias Mecanicas (ISSN 0100-7386*, vol. 16, pp. 205–211, 1994.

[2] H. P. P. Pereira, N. Violante-Carvalho, I. C. M. Nogueira, A. Babanin, Q. Liu, U. F. de Pinho, F. Nascimento, and C. E. Parente, "Wave observations from an array of directional buoys over the southern brazilian coast," *Ocean Dynamics*, vol. 67, pp. 1577–1591, 2017.

[3] P. J. Teunissen and O. Montenbruck, *Springer handbook of global navigation satellite systems*. Springer, 2017, vol. 10.

[4] S. S. Gao, Q. Luo, and F. Zhu, *Circularly polarized antennas*. John Wiley & Sons, 2013.

[5] S. Caizzone, M.-S. Circiu, W. Elmarissi, and C. Enneking, "All-GNSS-band DRA antenna for high-precision applications," in *12th European Conference on Antennas and Propagation (EuCAP 2018)*. IET, 2018, pp. 1–4.

[6] D. Nascimento, J. Mores, R. Schildberg, and J. da S Lacava, "Low-cost truncated corner microstrip antenna for GPS application," in *2006 IEEE Antennas and Propagation Society International Symposium*. IEEE, 2006, pp. 1557–1560.

[7] R. Garg, *Microstrip antenna design handbook*. Artech house, 2001.

[8] I. Singh, V. Tripathi *et al.*, "Microstrip patch antenna and its applications: a survey," *Int. J. Comp. Tech. Appl*, vol. 2, no. 5, pp. 1595–1599, 2011.

[9] R. K. Mongia and P. Bhartia, "Dielectric resonator antennas—A review and general design relations for resonant frequency and bandwidth," *International Journal of Microwave and Millimeter-Wave Computer-Aided Engineering*, vol. 4, no. 3, pp. 230–247, 1994.

[10] A. Petosa, S. Thirakounc, M. Zuliani, and A. Ittipiboon, "Comparison between planar arrays of perforated dras and microstrip patches," in *2005 IEEE Antennas and Propagation Society International Symposium*, vol. 2. IEEE, 2005, pp. 168–175.

[11] A. Kishk, K. Lee, D. Kajfez *et al.*, "Performance comparisons between dielectric resonator antennas and printed microstrip patch antennas at x-band." *Microwave Journal*, vol. 49, no. 1, 2006.

[12] Q. Lai, G. Almpanis, C. Fumeaux, H. Benedickter, and R. Vahldieck, "Comparison of the radiation efficiency for the dielectric resonator antenna and the microstrip antenna at ka band," *IEEE Transactions on Antennas and Propagation*, vol. 56, no. 11, pp. 3589–3592, 2008.

[13] R. Mongia, "Reduced size metallized dielectric resonator antennas," in *IEEE Antennas and Propagation Society International Symposium 1997. Digest*, vol. 4. Cambridge/Canada: IEEE, 1997, pp. 2202–2205.

[14] C.-Y. Huang, J.-Y. Wu, and K.-L. Wong, "Cross-slot-coupled microstrip antenna and dielectric resonator antenna for circular polarization," *IEEE Transactions on Antennas and Propagation*, vol. 47, no. 4, pp. 605–609, 1999.

[15] H. R. S. Rodrigues, E. R. Schlosser, and M. V. T. Heckler, "Antena de microfita de baixo custo e elevada eficiência para aplicações em GPS," in *21º Simpósio Brasileiro de Micro-Ondas e Optoeletrônica - (SBMO)*, 2024, pp. 1–5.